HIGHLY SOLAR ACTIVE Fe$_2$(MoO$_4$)$_3$ NANOCATALYST ASSISTED DEGRADATION OF RHODAMINE-B DYE

S. Tamilarasi[1], K. Balakrishnan*[1], I. Muthuvel[2,3], T. Rajachandrasekar[3], K. Gowthami[2], G. Thirunarayanan[2]

[1]*AVVM Sri Pushpam College (Autonomous), Poondi, Thanjavur, Tamil Nadu, India*
[2]*Department of Chemistry, Annamalai University, Annamalainagar, Tamil Nadu, India*
[3]*Department of Chemistry, MR Government Arts College, Mannargudi, Tamil Nadu, India*
*Corresponding author: professorkbavvm63@gmail.com

ABSTRACT

The hetero-Fenton catalyst Fe$_2$(MoO$_4$)$_3$ was prepared by simple co-precipitation method and it was characterized using X-ray diffraction (XRD), Fourier transform infrared spectroscopy (FT-IR), UV-visible diffuse reflectance spectroscopy (UV-vis-DRS) and field-emission scanning electron microscopy (FE-SEM) with energy dispersive X-ray spectroscopy (EDX). Fe$_2$(MoO$_4$)$_3$ was used for hetero-Fenton photocatalyst for the degradation of Rhodamine-B (Rh-B) under solar light. The effect of various operational parameters like catalyst concentration, initial solution pH, H$_2$O$_2$ dosage, initial dye concentration reusability on photodegradation were investigated and the optimum conditions are reported.

Keywords: Heterogeneous photo-Fenton, wastewater treatment, Rhodamine-B, Solar light

1. INTRODUCTION

Discarding recalcitrant pollutants from industrial effluents is the most non-trivial problem of the present era. Classical environmental technologies, which involves the separation of organic pollutants from wastewater result in the formation of toxic residues turns out to be a challenge. To circumvent this difficulty, advanced oxidation technologies (AOTs) were evolved which entwines the *in situ* generation of highly potent chemical oxidant OH radical represent an important class of environmental technologies [1-5]. Numerous techniques such as adsorption on activated carbon [6, 7], ozonization [8], electrochemical treatment [9], semiconductor photocatalysis [10, 11] and Fenton [12] etc., have been arrived into picture. Among the aforementioned technologies photo-Fenton process remain elegant because it is economical and can oxidatively degrade hydroxyl radical present in organic pollutants. Despite of this, the formation of sludge and usability in a narrow range of pH 2-3 stays as a disadvantage of homogeneous-Fenton process. Later on, heterogeneous-Fenton processes were adopted to furnish wide pH range, no sludge formation and the possibility to recycle the iron promoter. The efficiency of the process can be enhanced by irradiation of visible light,

because the photoreduction of Fe^{3+} promotes Fe^{2+} regeneration [13-16]. Diverse heterogeneous-Fenton catalysts such as Fe$_2$O$_3$ [17], Fe$_3$O$_4$ [18], FeOOH [19] and BiFeO$_3$ [20] have been already found in literature. In order to increase the efficiency of hetero-Fenton process various supports have been incorporated including zeolite [21], nafion [22], layered clay [23, 24] and cation exchange resin [25].

In the present work, we have adopted a metal molybdate nanoparticle as a catalyst which shows some unique properties and wide applicability in energy storage, gas sensing and catalysis. Succinctly, Fe$_2$(MoO$_4$)$_3$ has been incorporated as hetero-Fenton catalyst for the degradation of a well-known organic dye *viz.*, Rhodamine-B (Rh-B) under natural sunlight irradiation in the presence of H$_2$O$_2$. The structural studies of the catalyst have been accomplished using XRD, FT-IR, UV-Vis-DRS and FE-SEM with EDX analysis. The effect of catalysts loading, initial solution pH level, effect of H$_2$O$_2$ dosage, effect of initial dye concentration and effect of reusability on the degradation of Rh-B were extensively investigated. We had found that the replacement of OH radicals takes place in a shorts time in the presence of sunlight.

2. EXPERIMENTAL

2.1. Material and methods

Double distilled water was used for all dilution and sample preparation Rhodamine-B (C.I. 45170) was obtained from Himedia chemical, ammonium heptamolybdate $((NH_4)_6Mo_7O_{24}\cdot 4H_2O)$ (A.R), sodium hydroxide (NaOH) from Merck, ethanol (C_2H_5OH) and sulfuric acid (H_2SO_4) from Qualigens were used as received. The pH of the solution was adjusted using H_2SO_4 or NaOH.

2.2. Synthesis of iron molybdate ($Fe_2(MoO_4)_3$)

About 0.025 M of ammonium heptamolybdate $((NH_4)_6Mo_7O_{24}\cdot 4H_2O)$ in 50 mL distilled water was added drop wise into 0.05 M ferric chloride ($FeCl_3$). The above mixture was maintained at 80°C under continuous stirring. A light green precipitate was formed by adding sodium hydroxide solution to this mixture its pH adjusted to 7-8 on further stirring for 4 h. The precipitate was washed with distilled water and ethanol for several times. The sample was filtered and dried in oven at 80°C for 2 h. Then it was calcined in muffle furnace at 550°C for 6 h. Iron molybdate ($Fe_2(MoO_4)_3$) was obtained in the form of greenish powder.

2.3. Photocatalytic activity

For all the solar photo reacting experiment, 50 mL of dye solution containing appropriate quantity of the $Fe_2(MoO_4)_3$ suspension was used. The suspension was stirred for 30 min in the dark and then irradiated. The solution and dark dye was continuously aerated by a pump to provide oxygen and for complete mixing of reaction medium, sample for analysis were 2-3 mL extracted through pipette every 10 min and centrifuged immediately to separate the catalyst. The centrifugate (1 mL) was diluted to 10 mL and its absorbance was measured at 553 nm using UV-Vis spectrophotometer to determine the concentration of dye. From the concentration of dye during the degradation process, percentage of dye remaining was determined.

Heterogeneous photocatalytic degradation of Rh-B on iron immobilized catalyst was reported to follow *pseudo*-first order kinetics. At low initial dye concentration, the rate expression is given by $d[C]/dt = k'[C]$ where k' is the *pseudo*-first order rate constant. The dye was adsorbed on the catalyst surface and adsorption-desorption equilibrium was reached in 10 min after adsorption.

The equilibrium concentration of the solution was determined and taken as the initial dye concentration (C_0) for kinetic analysis. At $C = C_0$, t = 0, $\ln(C_0/C) = k't$, where C_0 is the equilibrium concentration of dye and C is the concentration at time t, *pseudo*-First order rate constant k' was determined from the plot of $\ln(C_0/C)$ *versus* t.

2.4. Solar experiment

All solar photocatalytic experiments were carried out in a open space on sunny days of summer under clear skies between 11 a.m and 2 p.m. Solar light intensity was measured for every 10 min and the average light intensity over the duration of each experiment was calculated of the sensor was always set at the position of maximum intensity. The intensity of solar light was measured using LT Lutron LX -10/A digital Lux meter. The intensity of solar light (1250 × 100 Lux) was nearly constant during the experiments.

2.5. Characterization of photocatalyst

X-Ray diffraction pattern was recorded on the Equinox-1000 model X-ray diffractometer from analytical instruments operated at a voltage of 30 kV and a current of 30 mA with $CuK\alpha$ (1.54056 Å). FT-IR spectrum was recorded using Shimadzu IRAffinity-1 spectrometer in KBr pellet. About 5 mg of sample was mixed with 50 mg of IR grade KBr, ground and pressed using hydraulic press under a pressure of 15 tons into wafer of 13 mm diameter. This pellet was used to record the infrared spectra in the range of 4000-400cm^{-1}.

The spectrum was recorded as percentage transmittance against wave number. The UV-DRS spectrum was recorded by using the instrument Jasco (Model No. V-670). FE-SEM images were taken using on Carl ziess-Specification EV018 scanning electron microscope. Samples were mounted on a carbon platform placed in the scanning electron microscope for taking images at various magnifications. EDX (Bruker-X-Flash X130) and elemental colour mapping were performed at different points of the surface in order to minimize any possible anomalies arising from the heterogeneous nature of the analyzed surface. Most elements were detected with the concentration in the order of 0.1%. Ultraviolet and visible light absorbance spectra were measured over a range of 200-700 nm with a Shimadzu UV-1650PC recording spectrometer using a quartz cell with 10 mm optical path length.

3. RESULTS AND DISCUSSION

3.1. Powder XRD analysis

The powder X-ray diffraction pattern was obtained for the prepared iron molybdate nanoparticles (Fig. 1). The crystalline peaks were indexed and were found to be in good agreement with the standard orthorhombic structure of $Fe_2(MoO_4)_3$ [26, 27] as per the standard JCPDS Card No. 85-2287 [28]. Further, the average crystalline size of the material was calculated by using the Scherrer's formula,

$$D = 0.9\lambda/\beta \cos\theta$$

Where, D is the average crystalline size of the material, β is the full width at half maximum (FWHM) of the crystalline peak of the particular plane, θ is the angle at which the crystal plane diffracts, and λ is the wavelength of the X-ray source used. Thus crystalline size was calculated by the above said Scherrer's equation and found to be 51.41 nm, Further the dislocation density is calculated using the formula, $\delta = 1/D^2$ and thus determined dislocation density was 3.7836×10^{-4}.
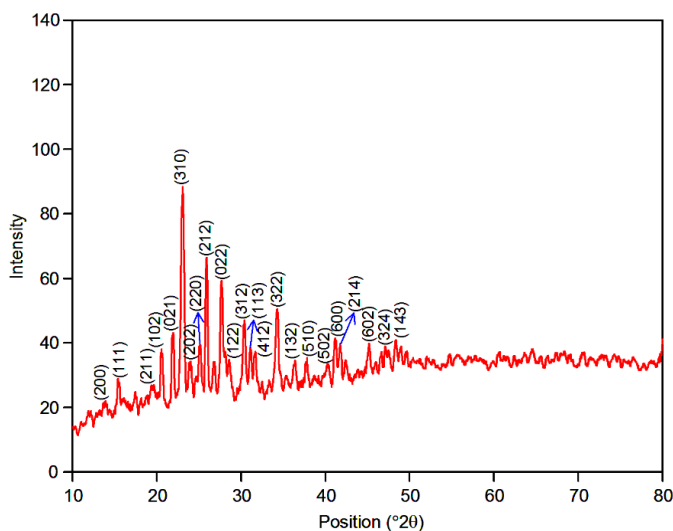

Fig. 1: XRD pattern of $Fe_2(MoO_4)_3$

3.2. FT-IR spectrum

The FT-IR analysis was used to investigate the surface structure and make insights into chemical bond. The recorded spectrum range was 4000-400 cm^{-1}. The FT-IR spectrum of $Fe_2(MoO_4)_3$ is shown in Fig. 2. The broad band was observed in the range of 1000-400 cm^{-1}. The characteristic band observed at 3291 cm^{-1} can be assigned to the stretching of O–H band due to the surface hydroxyl group present in the nanoparticles. The vibrational Mo–O bond 543 cm^{-1} non-equivalent tetrahedral Mo_4 unit in $Fe_2(MoO_4)_3$ and the bond located

is associated with the bridging Mo–O–Mo bond [27,29]. Narrow peak at 960 cm^{-1} was due to the stretching vibration of bridge oxygen atom of Fe–O–Mo. The absorption band around 600 cm^{-1} was assigned to Fe–O vibration [30].
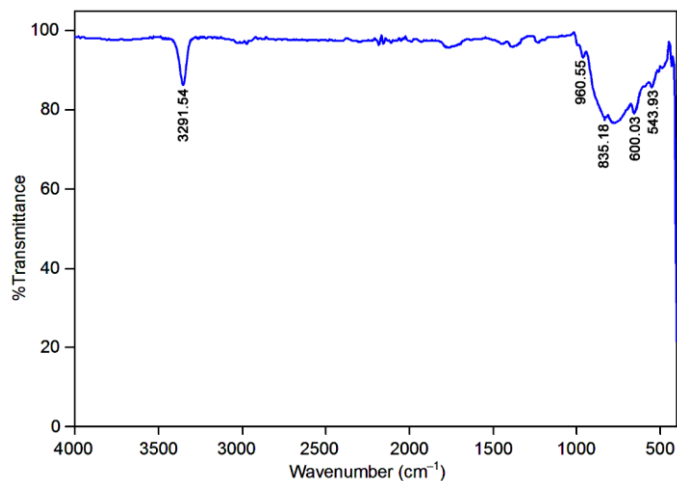

Fig. 2: FT-IR spectrum of $Fe_2(MoO_4)_3$.

3.3. UV–Vis-DRS

The UV-visible diffuse reflectance spectrum was taken to elucidate the optical properties of the synthesized material. The optical absorption was measured in the UV-visible region and the spectrum is shown in Fig. 3. The band absorption around 420-530 nm attributing to the excitation of electrons from the valence band to conduction band. By applying Kubelka-Munk function [31], from the Tauc plot $[F(R)h\nu]^2 Vs \ h\nu$ (eV), the direct band gap energy of the specimen is estimated as 2.29 eV (inset in Fig. 3).
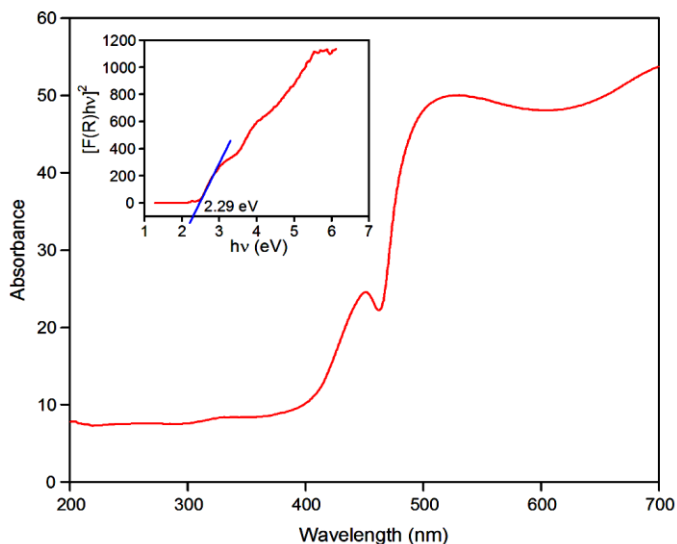

Fig. 3: UV-DRS absorbance spectrum of Fe2(MoO4)3 (Tauc plot in inset).

3.4. FE-SEM, EDX with Elemental Color Mapping

The surface morphology of the synthesized product was identified by FE-SEM measurements. Figs. 4a and 4b show the FE-SEM images of $Fe_2(MoO_4)_3$ needle like structure. The particles are uniformly distributed. Although the sizes of the particles are in few hundred nm (Fig. 4b), and some of the particle's sizes are in the range from 30 to 50 nm (Fig. 4a). The elemental compositional analysis has been characterized using EDX (Fig. 4c) and coupled with color mapping (inset in Fig. 4c) manifests that the presence of Fe, Mo and O in the bulk of $Fe_2(MoO_4)_3$ nanocomposites.

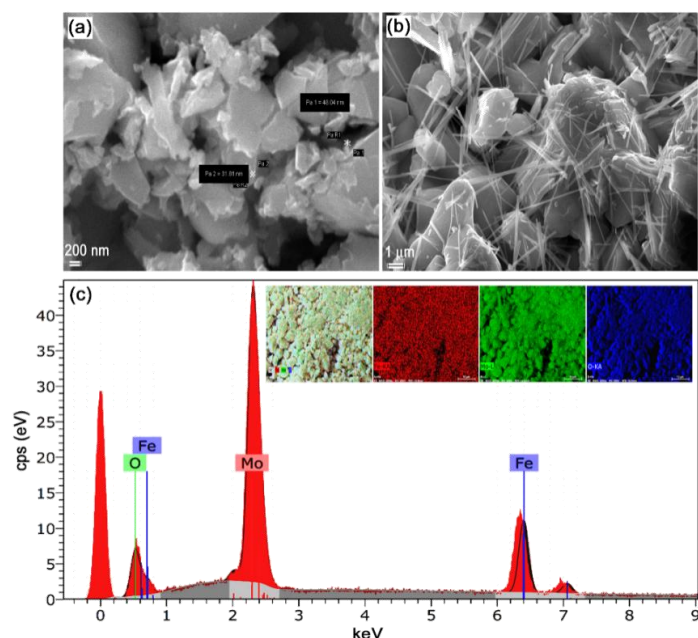**Fig. 4: FE-SEM images of $Fe_2(MoO_4)_3$: a) scale bar 200 nm, b) scale bar 1 μm and c) EDX of $Fe_2(MoO_4)_3$.**
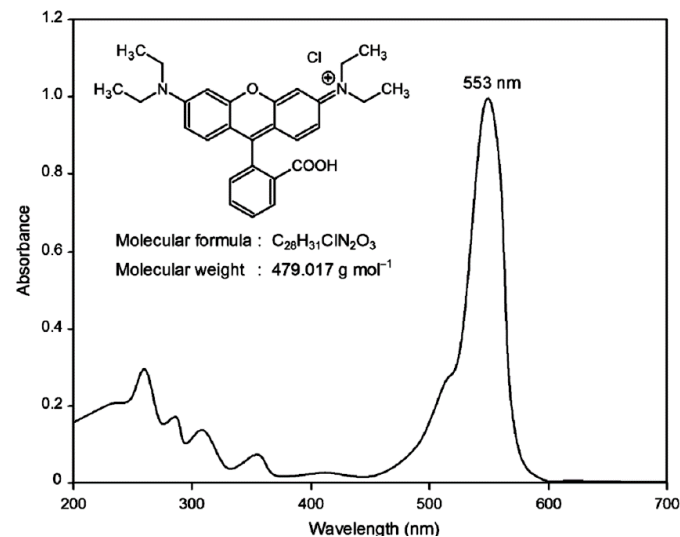

Fig. 5: Structure of Rh-B and its absorption spectrum. Absorbance maximum at 553 nm

3.5. Photocatalytic activity

The photocatalytic activities of $Fe_2(MoO_4)_3$ on the degradation of Rhodamine-B (Rh-B) under various conditions have been discussed. Structure and UV spectrum of the dye is given in Fig. 5.

3.6. Primary analysis

In the primary analysis, the degradation of Rh-B by the $Fe_2(MoO_4)_3$ catalyst under different conditions was evaluated by a batch of experiments. In Fig. 6, curve (a) represents dye is irradiated with solar light no small change in concentration was observed. In the presence of $Fe_2(MoO_4)_3$ dye is irradiated with solar light by only 10% of dye concentration decreased (curve b). Curve c is heterogeneous-Fenton type reaction (dye/$Fe_2(MoO_4)_3$/H_2O_2/solar), 99% degradation was observed at the time of 60 min. Curve d and f are dye on adsorption experiment in the presence of $Fe_2(MoO_4)_3$ with H_2O_2. In Curve e (dye/H_2O_2/solar) small percentage of dye concentration was observed.
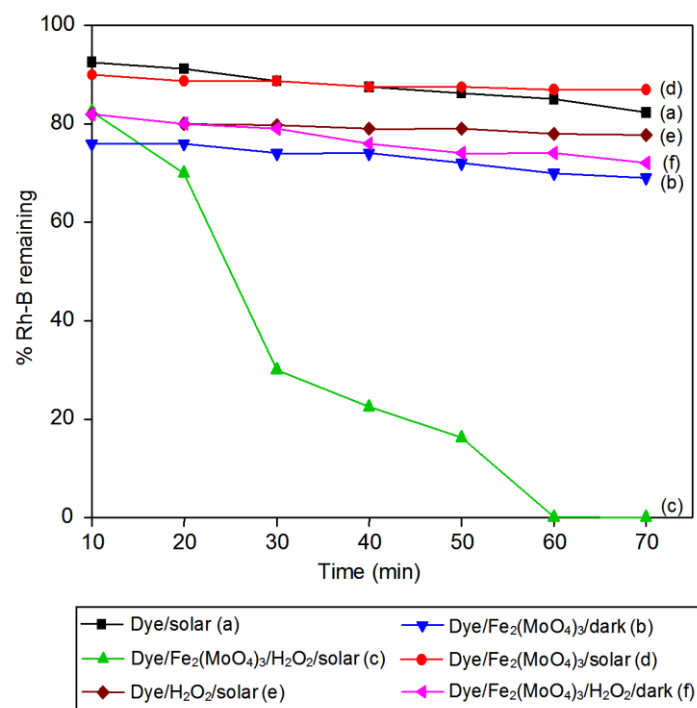
Fig. 6: Primary analysis of Rh-B under solar light. [Rh-B] = 5×10^{-4} M, catalyst suspended = 0.125 g L^{-1}, H_2O_2 = 10 mmol, airflow rate = 8.1 mL s^{-1}, pH 7, I_{solar} = 1250×100 Lux

3.7. Effect of catalyst loading

The catalyst loading on decolorization efficiency varied from 0.025 to 0.0150 g L^{-1} (Fig. 7). The result indicates decolorization of Rh-B was influenced by the catalyst

loading. A large dye decolorization was observed increasing catalyst from 0.025 to 0.125 g L^{-1}. The rate constant ranges from 0.0093 to 0.0454 min^{-1} for degradation (40 min irradiation). Further increase of catalyst from 0.125 to 0.150 gL^{-1} shows decrease for degradation efficiency for the reaction excess of Fe^{3+} with H$_2$O$_2$ producing less reactive hydroxyl radical [32,33]. Thus, 0.125 g L^{-1} catalyst concentration was found to be the optimum concentration for maximum degradation efficiency.
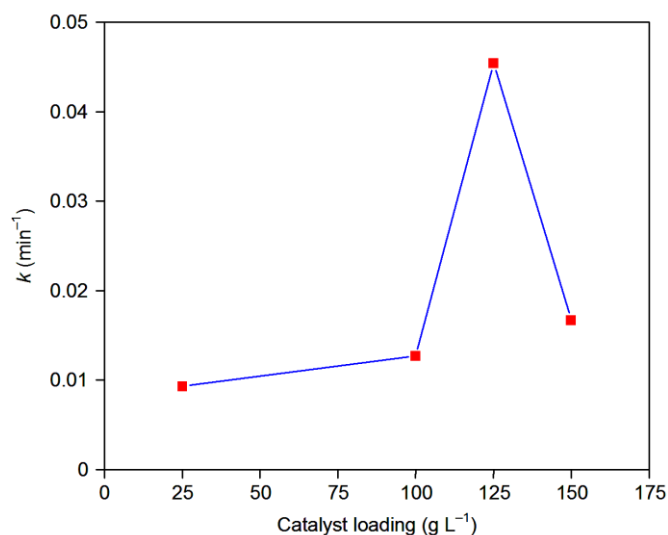
$$Fe^{3+} + H_2O_2 \xrightarrow{h\nu} Fe^{2+} + HO_2^\bullet + H^+ \qquad (1)$$

Fig. 7: Effect of catalyst loading. [Rh–B] = 5×10^{-4} M, H$_2$O$_2$ = 20 mmol, airflow rate = 8.1 mL s^{-1}, pH 7, irradiation time = 40 min,I_{solar} = 1250×100 Lux
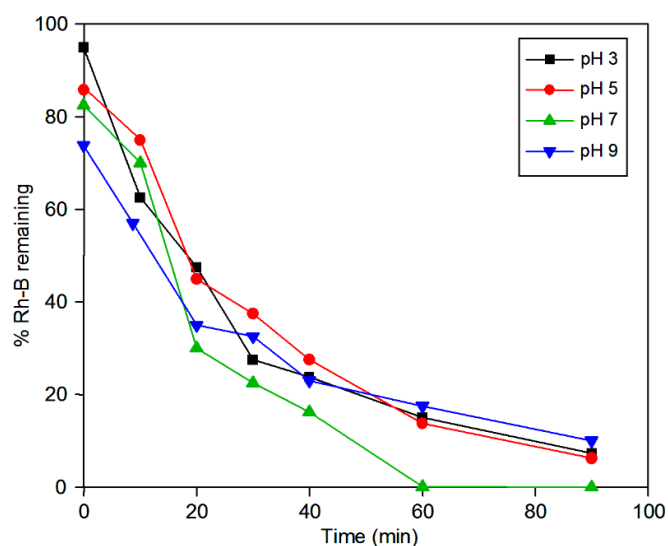
Fig. 8: Effect of initial solution pH. [Rh–B] = 5×10^{-4} M, catalyst suspended = 0.125 g L^{-1}, H$_2$O$_2$ = 20 mmol, airflow rate = 8.1 mL s^{-1}, irradiation time = 40 min,I_{solar} = 1250×100 Lux

The solution of pH plays a key role in advanced degradation process. Previous photocatalytic degradation studies indicate that pH affect photocatalytic process. The experiments were carried out at various pH values, ranging from 3 to 9 with constant amount of dye i.e. 5 × 10^{-4} M and catalyst 0.125 g L^{-1}. The evolution of the degradation efficiency with treatment of various pH 3, 5, 7 and 9 are shown in Fig. 8. About 76, 73, 84, 77% of Rh-B was degraded in 40 min for pH 3, 5, 7 and 9, respectively. Maximum degradation efficiency was observed at neutral pH. Hence, pH 7 was considered as optimum pH for further studies. [34].

3.9. Effect of H$_2$O$_2$ dosage
The initial concentration of H$_2$O$_2$ is an important parameter for the degradation of the dye in the heterogeneous photo-Fenton reaction.
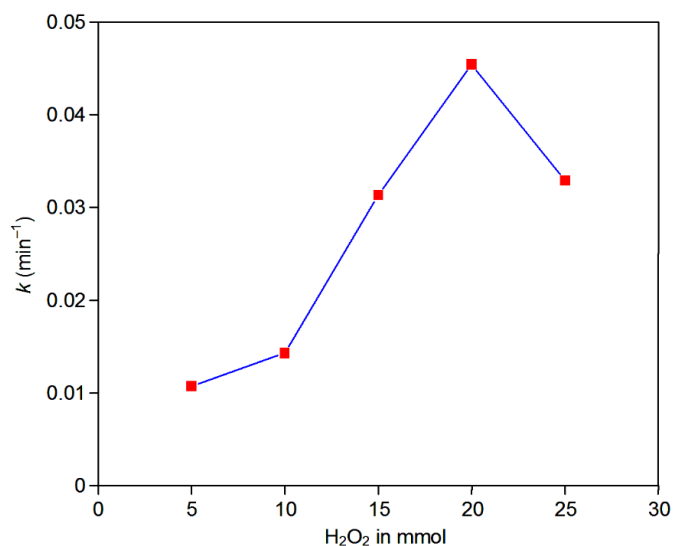

Fig. 9: Effect of H$_2$O$_2$ dosage. [Rh–B] = 5×10^{-4} M, catalyst suspended = 0.125 g L^{-1}, airflow rate = 8.1 mL s^{-1}, pH 7,irradiation time = 40 min,I_{solar} = 1250×100 Lux

Fig. 9 illustrates decolourization of Rh-B at different H$_2$O$_2$ hydrogen peroxide concentrations. The photolysis of Rh-B with Fe$_2$(MoO$_4$)$_3$ at pH 7 different concentrations of H$_2$O$_2$ (5-25 mmol) increases *pseudo*-first order rate constant from 0.0107 to 0.0454 min^{-1} in the degradation time of 40 min^{-1}. At low concentration (5-10 mmol) H$_2$O$_2$ generates hydroxyl radicals and the decolourization efficiency was slow. The increase of hydrogen peroxide (10-20 mmol) concentration would lead to more hydroxyl radical introduced. Hence 20 mmol of H$_2$O$_2$ is the optimal level for decolourization by

addition of H_2O_2 is due to increased production of hydroxyl radical.

$$H_2O_2 + e_{CB-} \rightarrow {}^\bullet OH + OH^- \qquad (2)$$

$$H_2O_2 + O_2^{\bullet-} \rightarrow {}^\bullet OH + OH^- + O_2 \qquad (3)$$
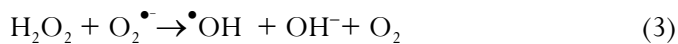
At concentration above 20 mmol, the removal rate decreases due to production of hydroperoxyl radical $(HO_2^\bullet)$. In the presence of excess (H_2O_2) and hydroperoxy radical less reactive do not contribute to oxidation addition [21, 35].

$$H_2O_2 + {}^\bullet OH \rightarrow HO_2^\bullet + H_2O \qquad (4)$$
$$HO_2^\bullet + {}^\bullet OH \rightarrow H_2O + O_2 \qquad (5)$$

3.10.   Effect of initial dye concentration

At a fixed weight of $Fe_2(MoO_4)_3$ and pH, H_2O_2 the effect of initial dye concentration ranged 1 to 6×10^{-4} M on decolourization of Rh-B dye by photo-Fenton degradation under solar light. Increase of the initial dye concentration rate constant from 40 min^{-1} (Fig. 10) at higher initial dye concentration but constant concentration of $^\bullet OH$ radicals, the relative concentration of radical was lower. In photo-Fenton process at higher dye concentration the penetration of photon entering into solution also decrease, which led to decreased decolorization efficiency [12, 36, 37].
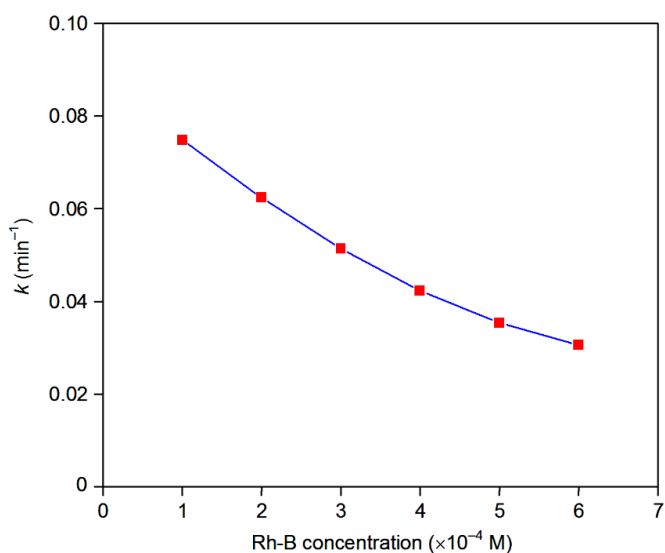

Fig. 10: Effect of initial dye concentration. Catalyst suspended = 0.125 g L^{-1}, H$_2$O$_2$ = 20 mmol, airflow rate = 8.1 mL s^{-1}, pH 7, irradiation time = 40 min, I_{solar} = 1250×100 Lux

3.11.   Effect of long-term stability

The long-term stability of the heterogeneous photo-Fenton catalyst was tested and the results are shown in Fig. 11. About 89% dye removal takes place at 60 min in the first run. The same catalyst was separated, dried and used again. In the second run 89% of dye was removed at 60 min. Third run gave 88% of dye removal. After third run the catalyst was stable and no significant change was observed in efficiency. It indicates the catalyst is reused without loss of activity.
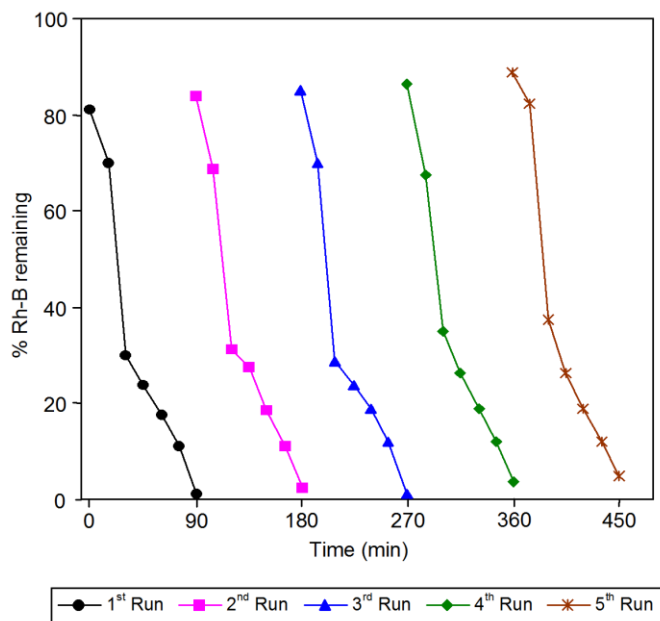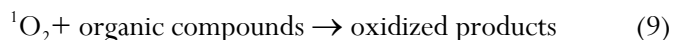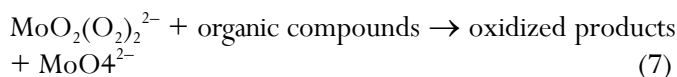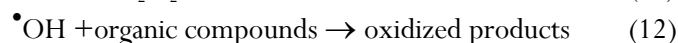

Fig. 11: Effect of long-term stability. [Rh-B] = 5×10^{-4} M, catalyst suspended = 0.125 g L^{-1}, H$_2$O$_2$ = 20 mmol, airflow rate = 8.1 mL s^{-1}, pH 7, I_{solar} = 1250×100 Lux

3.12.   Mechanism

The mechanism involves the formation of molybdenum (Mo) peroxo complex, such as $MoO_3(O_2)^{2-}$, $MoO_2(O_2)_2^{2-}$, $MoO(O_2)_3^{2-}$ or $Mo(O_2)_4^{2-}$ (eqn. 6), which is a strong oxidant and can oxidize the organic compounds by the direct oxygen transfer (eqn. 7) [38] or by the singlet oxygen ($^1O_2$) generated from the peroxo complex (eqns. 8 and 9) [39].

$$MoO_4^{2-} + 2H_2O_2 \rightarrow MoO_2(O_2)_2^{2-} + 2H_2O \qquad (6)$$

$$MoO_2(O_2)_2^{2-} + \text{organic compounds} \rightarrow \text{oxidized products} + MoO4^{2-} \qquad (7)$$

$$MoO_2(O_2)_2^{2-} \rightarrow MoO_4^{2-} + {}^1O_2 \qquad (8)$$

$${}^1O_2 + \text{organic compounds} \rightarrow \text{oxidized products} \qquad (9)$$

It is popularly believed that the mechanism of the Fe^{3+}/H_2O_2 system involves the reduction of Fe^{3+} to Fe^{2+} (eqn. 10). The formed Fe^{2+} then reacts with H_2O_2 to generate $^\bullet OH$ radicals (eqn. 11), which are ready to degrade the organic compounds (eqn. 12) [40].

$$=Fe^{3+} + H_2O_2 \rightarrow =Fe^{2+} + {}^\bullet OOH + H^+ \qquad (10)$$

$$=Fe^{3+} + H_2O_2 \rightarrow =Fe^{3+} + {}^\bullet OH + OH^- \qquad (11)$$

$${}^\bullet OH + \text{organic compounds} \rightarrow \text{oxidized products} \qquad (12)$$

In order to clarify if Fe^{3+} and MoO_4^{2-} in $Fe_2(MoO_4)_3$ independently activated H_2O_2 or there is any synergistically catalytic effect between them, we carried out comparable experiments using various Fenton-like catalysts. It suggests that there is a synergistically catalytic effect between Fe^{3+} and MoO_4^{2-} in the compound.

4. CONCLUSION

Degradation of Rhodamine-B (Rh-B) was studied in detail using solid acid $Fe_2(MoO_4)_3$ as a heterogeneous Fenton-like catalyst. The results showed that $Fe_2(MoO_4)_3$ can effectively activate H_2O_2 to degrade Rh-B and the efficiency is slightly affected by pH of the solution in the range of 3, 5, 7 and 9. Hence, $Fe_2(MoO_4)_3$ show high catalytic activity towards degradation of Rh-B. The role of molybdenum in $Fe_2(MoO_4)_3$ mainly includes two aspects: i) MoO_4^{2-} itself can activate H_2O_2 to degrade Rh-B by the direct oxygen transfer or by the singlet oxygen ($^1O_2$) pathway. Moreover, $Fe_2(MoO_4)_3$ exhibited low iron leaching, good structural stability and no loss of performance after five recycle times. These experimental results present a new clue to develop highly active heterogeneous Fenton-like catalysts at neutral pH.

5. REFERENCES

1. Reisch MS. *Chem Eng News*, 1988; **66:**7-14.
2. Hoffmann M R, Martin S T, Choiand W, Bahnemann DW. *Chem Rev,* 1995; **95:** 69-96.
3. Rai HS, Bhattacharya MS, Singh J, Bansal TK, Vats P, Banerjee UC. *Crit Rev Environ Sci Technol,* 2005;**35:** 219-238.
4. Baldez EE, Robaina NF,Cassella RJ. *J Hazard Mater*, 2008; **159:** 580-586.
5. Vogelpohl A, Kim SM. *J Ind Eng Chem*, 2004; **10:**33-40
6. KhoslaE, KaurS, DaveP N. *J Chem Eng Data,* 2012; **57:**412-419.
7. MallI D, Srivastava VC, Agarwal NK. *Dyes Pigments,*2006;**69:**210-223.
8. Wu J, Doan H, Upreti S. *Chem Engg J*, 2008; **142:**156-160.
9. RochaJHB, Solano AMS, Fernandes NS, Da Silva DR, Peralta-Hernandez JM, Martinez-Huitle CA. *Electrocatalysis,*2012; **3:**1-12.
10. Sobana N, Muruganandham M, Swaminathan M. *J Mol Catal A*, 2006; **258:**124-132.
11. Sobana N, Swaminathan M. *Sol Energy Mater Sol Cells,* 2007; **91:**727-734.
12. Muthuvel I, Swaminathan M. *Catal Commun,* 2007; **8:**981-986.
13. Fukushima M, Tatsumi K, Nagao S. *Environ Sci Technol,* 2001; **35:**3683-3690.
14. Klamerth N, Malato S, Maldonado MI, Aguera A, Fernandez-Alba AR. *Environ Sci Technol,* 2010; **44:**1792-1798.
15. Vermilyea AW, Voelker BM. *Environ Sci Technol,* 2009; **43:**6927-6933.
16. Gao Y, Gan H, Zhang G, Guo Y. *Chem Engg J,* 2013; **217:**221-230.
17. Feng J, Hu X,Yue PL. *Environ Sci Technol,* 2004; **38:**5773-5778.
18. Zhang J, Zhuang J, Gao L, Zhang Y, Gu N, Feng J, et al. *Chemosphere,* 2008; **73:**1524-1528.
19. Li Y, Zhang FS. *Chem Engg J,* 2010; **158**:148-153.
20. Luo W, Zhu LH, Wang N, Tang H, Cao M, She Y. *Environ Sci Technol,* 2010; **44:**1786-1791.
21. Neamtu M, Catrinescu C,Kettrup A. *Appl Catal B,* 2004; **51**:149-157.
22. Sabhi S, Kiwi J. *Water Res,* 2001; **35:**1994-2002.
23. Mosteo R, Ormad P, Mozas E, Sarasa J, Ovellerio J L. *Water Res,*2006; **40:**1561-1568.
24. Sum OSN, Fen J, Hu X, Yue PL. *Chem Engg Sci,* 2004; **59:**5269-5275.
25. Lv X, Xu Y, Lv K, Zhang G. *J Photochem Photobiol A,* 2005; **173:**121-127.
26. Pardehkhorram R, Tajarodi A, Imani M, Ebrahimi S, Koshy P, Sorrell CC, *J Aust Ceram Soc,* 2015; **51:**94-98.
27. Ramachandran R, Chidambaram S, Baskaran, Muthukumarasamy A, Lawrence JB. *BullMater Sci,* 2017; **40:**87-92.
28. Ding Y, Yu SH, Liu C, Zang ZA. *Chem Eur J,* 2007; **13:**746-753.
29. Soraes AP V, Portela MF, Kiennemann A, Hilaire L, Millet JMM. *Appl Catal A,* 2001; **206:**221-229.
30. Belhekar AA, Ayyappan S, Ramaswamy AV. *J Chem Technol Biotechnol,* 1994; **59:**395-402.

31. Kubelka P, Munk F. *Zeitschrift Technische Physik*, 1931; **12:**593-601.

32. Kwan CY, Chu W. *Water Res,* 2003; **37**:4405-4412.

33. Muthuvel I, Swaminathan. *Sol Energy Mater Sol Cells,* 2008; **92:**857-863.

34. Tian SH, Tu YT, Chen DS, Chen X, Xiong Y. Chem*Engg J,* 2011; **169:**31-37.

35. Buxton GV, Greenstock CL, Helman WP, Ross AB. *J Phys Chem Ref Data,* 1988; **17:**513-886.

36. Sun SP, Li CJ, Sun JH, Shi SH, Fan MH, Zhou Q. *J Hazard Mater,* 2009; **161:**1052-1057.

37. Ji F, Li C, Zhang J, Deng L. J *Hazard Mater,* 2011; **186**:1979-1984.

38. Shi HC, Wang XY, Hua RM, Zhang ZG, Tang J. *Tetrahedron,* 2005; **61:**1297-1302.

39. Linand JM, Liu ML. *Spectrochim. Acta A,* 2009; **72:**126-132.

40. Kwan WP, Voelker BM. *Environ Sci Technol,* 2003; **37:**1150-1158.